nature physics

ARTICLES

PUBLISHED ONLINE: 24 APRIL 2011 | DOI: 10.1038/NPHYS1983

Controlled near-field enhanced electron acceleration from dielectric nanospheres with intense few-cycle laser fields

Sergey Zherebtsov[1†], Thomas Fennel[2*†], Jürgen Plenge[3†], Egill Antonsson[3], Irina Znakovskaya[1], Adrian Wirth[1], Oliver Herrwerth[1], Frederik Süßmann[1], Christian Peltz[2], Izhar Ahmad[1], Sergei A. Trushin[1], Vladimir Pervak[4], Stefan Karsch[1,4], Marc J. J. Vrakking[5,6], Burkhard Langer[3], Christina Graf[3], Mark I. Stockman[1,7], Ferenc Krausz[1,4], Eckart Rühl[3*] and Matthias F. Kling[1,8,9*]

Collective electron motion in condensed matter typically unfolds on a sub-femtosecond timescale. The well-defined electric field evolution of intense, phase-stable few-cycle laser pulses provides an ideal tool for controlling this motion. The resulting manipulation of local electric fields at nanometre spatial and attosecond temporal scales offers unique spatio-temporal control of ultrafast nonlinear processes at the nanoscale, with important implications for the advancement of nanoelectronics. Here we demonstrate the attosecond control of the collective electron motion and directional emission from isolated dielectric (SiO_2) nanoparticles with phase-stabilized few-cycle laser fields. A novel acceleration mechanism leading to the ejection of highly energetic electrons is identified by the comparison of the results to quasi-classical model calculations. The observed lightwave control in nanosized dielectrics has important implications for other material groups, including semiconductors and metals.

The interaction of nanostructured materials with few-cycle laser light is at present attracting significant attention[1–3]. This interest is driven both by the quest for fundamental insight into the real-time many-electron dynamics and a wide range of applications, including ultrafast computation and information storage on the nanoscale[4], the generation of extreme ultraviolet (XUV) frequency combs[3], and plasmon-enhanced photoprocesses in femtosecond photochemistry, light detection, and solar energy conversion[5]. Access to the attosecond dynamics of nanostructured materials under laser light at optical frequencies became feasible with the availability of waveform-controlled near single-cycle optical fields[6] and XUV light pulses as short as 80 attoseconds[7,8]. Such light fields have made it possible to study tunnelling of electrons in atomic ionization[9], valence electron motion in atoms[10], attosecond photoemission dynamics in solids[11], and may serve to monitor nanolocalized plasmonic fields with attosecond temporal resolution[12].

The key to applications of nanosystems in the ultrafast regime is the control of nanoscopic electric fields on sub-cycle timescales[12]. A powerful tool to steer electron dynamics on sub-femtosecond timescales is the use of phase-controlled few-cycle laser pulses in the visible[13], where the electric field evolution is given by $E(t) = E_0(t)\cos(\omega t + \varphi)$, where $E_0(t)$ is the amplitude envelope, ω the angular frequency of the carrier wave, and φ the carrier-envelope phase (CEP). Waveform-controlled laser fields have been previously used to control the electron emission from atoms[14] and electron localization in molecules[15]. One of the most promising routes to the realization of electronics operating at light wave frequencies[8] arises from applying such waveform-controlled few-cycle light fields to nanoscale systems[16–18].

Recent theoretical work predicts efficient phase control of surface-plasmon driven electron emission from metallic nanofilms, where electrons are accelerated by the locally enhanced evanescent field of laser-induced surface-plasmons[18,19]. Also recollision of electrons in strong laser fields was shown to be important for nanosystems, for example for high-harmonic generation in clusters[20] and the fragmentation dynamics of C_{60} (ref. 21). High-energy electron emission observed recently in medium sized Ag clusters was ascribed to a rescattering process, where electrons are driven through the cluster by the plasmon-enhanced polarization field[22]. The present work focuses on dielectric nanoparticles in the gas phase and reports a novel phase-sensitive acceleration mechanism relying on electron backscattering from the surface of the nanoparticles in the presence of a dynamical near field. Dielectric nanoparticles were chosen as their spectral response is wide allowing the effective use of the full bandwidth of ultrashort pulses. Furthermore, the larger work function makes it possible to realize tunnelling ionization conditions with relatively low ionization yields up to high intensities, enabling the probing of the dielectric response with only limited interaction between liberated carriers. By imaging

[1]Max Planck Institute of Quantum Optics, Hans-Kopfermann-Str. 1, 85748 Garching, Germany, [2]Institute of Physics, University of Rostock, Universitätsplatz 3, 18051 Rostock, Germany, [3]Physical Chemistry, Freie Universität Berlin, Takustr. 3, 14195 Berlin, Germany, [4]Physics Department, Ludwig-Maximilian University, Am Coulombwall 1, 85748 Garching, Germany, [5]Max-Born-Institut, Max-Born Strasse 2A, D-12489 Berlin, Germany, [6]FOM Institute for Atomic and Molecular Physics, Science Park 113, 1098 XG Amsterdam, The Netherlands, [7]Department of Physics and Astronomy, Georgia State University, Atlanta, Georgia 30303, USA, [8]J.R. Macdonald Laboratory, Department of Physics, Kansas State University, Manhattan, Kansas 66506, USA, [9]King Abdullah Institute for Nanotechnology, King Saud University, Riyadh 11451, Saudi Arabia. [†]These authors contributed equally to this work. *e-mail: thomas.fennel@uni-rostock.de; ruehl@chemie.fu-berlin.de; matthias.kling@mpq.mpg.de.

the electron emission from 52 to 147 nm SiO_2 nanoparticles under intense ($1–4.5\times10^{13}$ W cm^{-2}) few-cycle (5 fs) waveform-controlled optical laser pulses, high kinetic energy electrons up to 100 eV and directional control of the electrons with the CEP are observed. Quasi-classical simulations reveal that electrons released from the nanoparticle surface are accelerated by the combined action of the dielectrically enhanced near field and the surface trapping potential produced by released electrons and residual ions, and reach maximum energy after backscattering from the nanoparticle surface at an optimal phase of the field. The combined near-field effects result in a strong suppression of direct electron emission and an increase of the electron energy cutoff of up to a factor of five over the classical atomic $10U_p$ cutoff law for backscattering, demonstrating the feasibility of manipulating phase-controlled rescattering processes by the local fields from nanostructured dielectric materials.

Electron emission from isolated nanoparticles

The laser-induced electron emission from isolated nanoparticles is studied in the gas phase to analyse their response properties free of any interactions with a substrate. The nanoparticles were prepared in a focused beam by applying aerodynamic focusing[23,24]. As every laser shot interacts with a fresh sample, ultrafast processes can be studied even up to conditions where the particles undergo Coulomb explosion after the interaction with the laser pulse. However, it is important to stress, that the short interaction time with the few-cycle laser field used in our experiment allows us to restrict the laser interaction with the particles to a few femtoseconds. This enables us to separate the laser-induced electron emission and acceleration from any electronic and nuclear dynamics taking place on longer timescales[25,26]. In this respect our set-up differs strongly from excitation schemes, where energetic electrons were observed from resonant plasmon excitation of strongly ionized, Coulomb exploding clusters and nanoparticles in femtosecond laser fields[22,27–29]. In this work, the nuclear motion can be considered frozen during the interaction of the laser with the nanoparticle. CEP-stabilized 5 fs laser pulses were generated as described in earlier work[30] and focused onto the nanoparticle beam. The resulting full 3D momentum distribution of emitted electrons was obtained from a velocity-map imaging (VMI) spectrometer. More details of the experimental set-up and methods are provided in the Supplementary Information.

Figure 1a shows a typical cut through the photoelectron momentum distribution ($p_z = 0$ plane) resulting from above-threshold ionization (ATI) of Xe atoms, which serves as a reference for the measurement on nanoparticles at the same intensity. The images are averaged over a 2π CEP range to increase the signal-to-noise ratio. The polarization axis of the laser is along the p_y-axis. The ATI signal in the momentum distribution is typically attributed to two principal mechanisms[31,32]: (1) direct electron emission and (2) electron (re)scattering. These two contributions can be distinguished from each other in the electron kinetic energy spectrum shown in Fig. 1b. The electrons at low energies below about 2–3 eV leave the atom directly, whereas a much smaller fraction of the electrons returns to the parent ion and (re)scatters, acquiring kinetic energies up to about 16 eV. The cutoff for the rescattered electrons in the classical limit is $10U_p$, where $U_p = e^2E_0{}^2/4m\omega^2$ is the ponderomotive potential of an electron in the laser field. Figure 1d shows the experimental momentum distribution of electrons emitted from 109 nm diameter SiO_2 nanoparticles at the same laser parameters. The angular distribution is more isotropic than that of Xe, and the corresponding photoelectron spectrum extends up to much higher kinetic energies of about 50 eV (see Fig. 1e).

For a few-cycle laser pulse the waveform of the laser field offers a possibility to control the electron emission directions by the CEP (ref. 33). The directional electron emission is expressed by the asymmetry parameter $A(W,\varphi) = (P_{up}(W,\varphi) - P_{down}(W,\varphi))/(P_{up}(W,\varphi) + P_{down}(W,\varphi))$ for the electron kinetic energy W and CEP φ, where $P_{up}(W,\varphi)$ and $P_{down}(W,\varphi)$ are the angle-integrated electron yields in the up (positive p_y momentum) and down (negative p_y momentum) directions. Figure 1c and f shows $A(W,\varphi)$ for Xe and SiO_2, respectively. Periodic oscillations of the asymmetry parameter with CEP are present in the energy range up to the cutoff of the asymmetry at (15.7 ± 0.5) eV for Xe and (49.6 ± 3.0) eV for SiO_2 (corresponding to $(54.1\pm4.4)U_p$), which is in good agreement with the spectral cutoffs. From the cutoff in the Xe data a laser pulse intensity of $(1.9\pm0.1)\times10^{13}$ W cm^{-2} is derived by comparison to the semi-classical cutoff formula of $10.007U_p + 0.538I_p$, where I_p is the ionization potential of Xe, given in ref. 34 and further verified by comparison of the experimental momentum distributions with results obtained by solving the time-dependent Schrödinger equation (TDSE), see Supplementary Information. The energy-dependent slopes in the asymmetry map of Xe are similar to those previously observed in atoms[35]. For SiO_2 the slopes are steeper and the asymmetry oscillations versus CEP cover a broad energy range up to the cutoff energy, with the strongest contributions above 10 eV. Laser-driven acceleration of these high energy electrons is supported by the observation of significant directional emission itself and by the fact that the asymmetry maxima versus CEP shift with energy. Because of the latter effect and the nearly linear scaling of the energy cutoff with intensity, as analysed in detail below, electron evaporation resulting from asymmetric heating of the nanoparticles can be excluded as the origin of these energetic electrons.

The experimental cutoff values in the kinetic energy spectra for differently sized nanoparticles and intensities studied here are shown in Fig. 2. The cutoff energy shows a nearly linear dependence on laser intensity, and an average cutoff value of $(53.0\pm0.6)U_p$ is obtained from a linear fit (black solid line in Fig. 2). Interestingly, no significant dependence of the electron energy cutoff on the particle size is observed within the experimental error bars. Only for spheres with diameters exceeding 200 nm do finite-difference time-domain (FDTD) calculations indicate that the field distribution inside the particles and the dielectric near-field enhancement close to the surface become substantially distorted by propagation effects, such as nanofocusing (see calculation results in the Supplementary Information).

Microscopic analysis of the electron emission

To model the nanoparticle ionization dynamics and the electron emission processes we use a quasi-classical trajectory-based Monte-Carlo approach. The removal of electrons from the nanoparticle surface and their subsequent classical propagation are considered to be driven by the effective field produced by the laser pulse, the nanoparticle polarization, and free charges. The last two contributions express the many-particle character of the target and lead to highly dynamical effective fields when compared to the atomic case. Both the initial ionization step and scattering processes of electrons that penetrate the nanoparticle are described stochastically by means of rate equations, in analogy to Monte-Carlo simulations for charge transport in bulk semiconductors[36]. The classical trajectories are interpreted as the centre-of-mass motion of the corresponding electronic quantum wavepackets. Interference effects, which are often described by quantum orbit theory[37] for atomic systems, are neglected, as the phase relations between different electron trajectories are nearly random in systems containing many active electrons. A large number of trajectories ($\sim10^6$) is propagated simultaneously within a statistical ensemble to evaluate the Coulomb mean-field term and the electron spectra. More details on the model are provided in the Supplementary Information.

The lower panels of Fig. 1 show the focal volume averaged momentum map, energy spectrum, and asymmetry map calculated for parameters close to the experiment. The calculated data reproduces the main experimental features, with featureless spectra

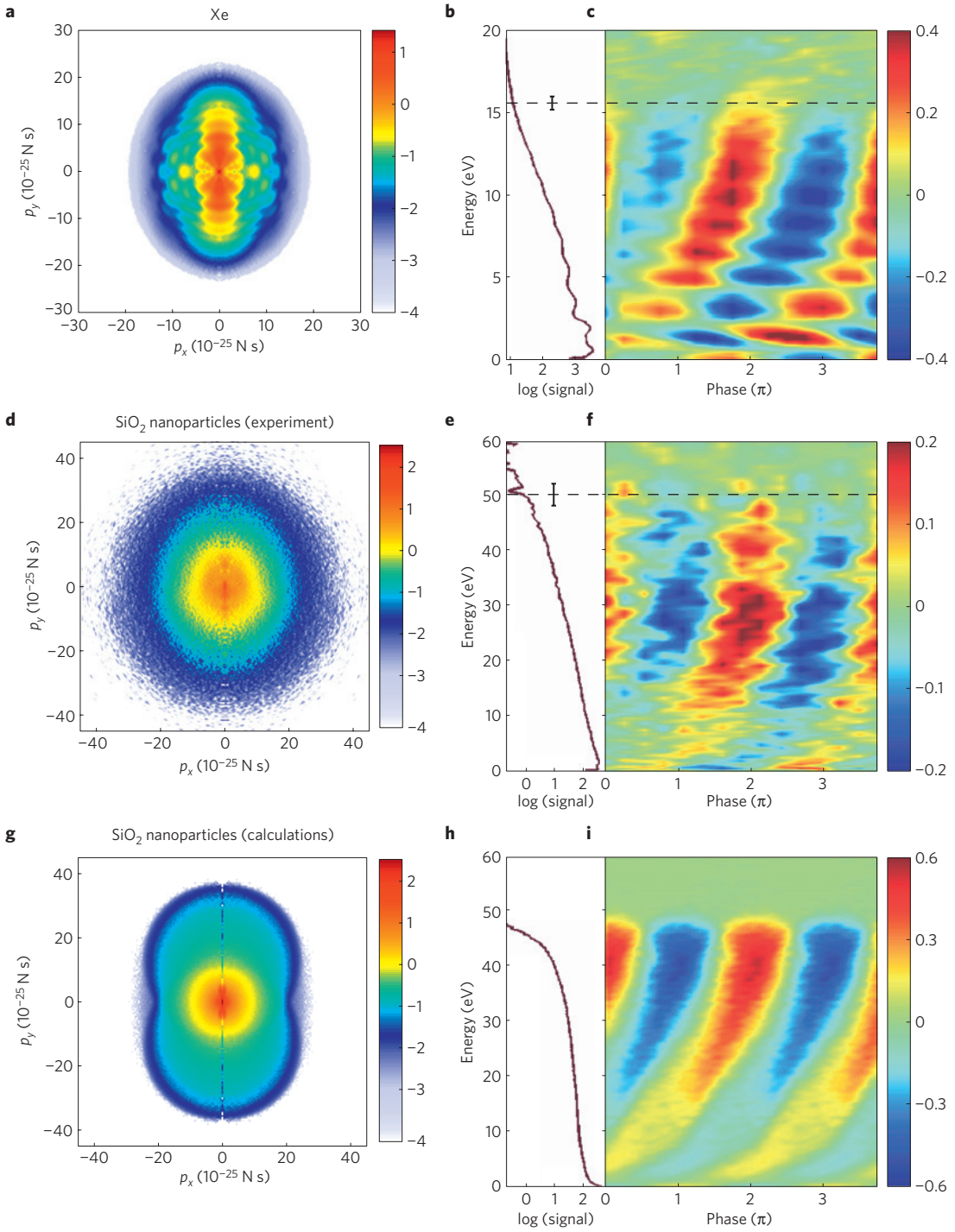

Figure 1 | Electron emission from Xe and SiO_2 nanoparticles. a, Momentum map of photoelectrons from Xe (log colour scale) at an intensity of 1.9×10^{13} W cm^{-2} averaged over the carrier-envelope phase with the laser polarization along the p_y axis. **b**, Electron kinetic energy spectrum obtained from angular integration of **a** over a 50° emission cone (full opening angle) along the laser polarization axis. **c**, Asymmetry of the electron emission from Xe as a function of the electron kinetic energy and phase. **d**, Momentum map of photoelectrons from SiO_2 nanoparticles of 109 ± 6 nm diameter (log colour scale) measured at the same conditions as the data shown in **a** for Xe. **e**, Electron kinetic energy spectrum obtained from angular integration of **c** over a 50° emission cone (full opening angle) along the laser polarization axis. **f**, Asymmetry of the electron emission from SiO_2 as a function of electron kinetic energy and phase. The standard deviation in the asymmetry was determined to be about 0.02 and 0.07 over the entire energy range for the measurements in Xe and SiO_2, respectively. The electron energy cutoff was defined as the position where the asymmetry amplitude approaches the background level (dashed lines). The vertical bars indicate the uncertainty of the cutoff energy, defined as the energy interval within which the asymmetry amplitude increases from the background level to two times this value. Results of the theoretical calculations. **g**, Momentum map of the electrons emitted from a SiO_2 nanosphere of 100 nm diameter (log colour scale) at an intensity of 2×10^{13} W cm^{-2}, averaged over the phase and the focal intensity distribution. The signal in the centre stems from directly emitted electrons, more energetic electrons originate from rescattering. **h**, Electron energy spectrum obtained by angular integration of **g** over a 50° emission cone (full opening angle) along the laser polarization axis. **i**, Corresponding asymmetry of the electron emission from SiO_2 versus electron kinetic energy and phase. A constant background signal equal to the signal at 40 eV has been assumed in the calculation. Note the different momentum and energy scales used for atoms and nanoparticles.

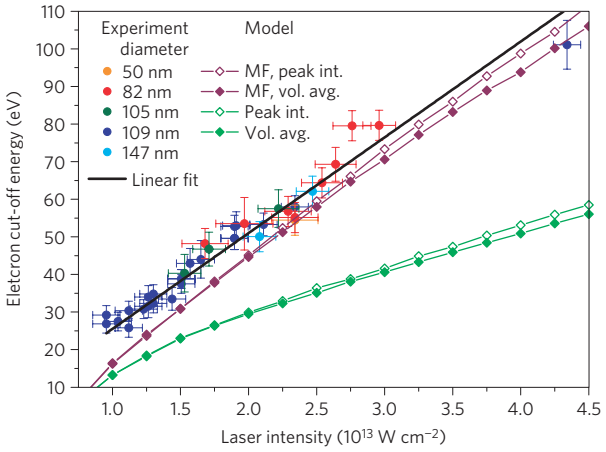

Figure 2 | Dependence of the cutoffs in the electron emission spectra from SiO_2 nanoparticles on laser intensity. The experimental results for nanoparticles of different sizes are represented by circles of different colours, as indicated in the legend. The experimental data are fitted by a linear function (black solid line) with a slope of $(53.0 \pm 0.6)U_p$. The cutoffs predicted for SiO_2 nanoparticles with 100 nm diameter by the simulations (see Fig. 3) with the laser and polarization fields only are shown as green lines, and calculations with the mean field (MF) included are shown as purple lines. For both types of curves, open diamonds correspond to single laser intensity calculations (peak int.) and filled diamonds correspond to volume averaged (vol. avg.) data. The latter accounts for the spatial intensity profile of the experimental laser focus. The error bars were determined from the uncertainties in the electron cutoff energies from Xe and SiO_2 nanoparticles, similar to the error bars given in Fig. 1.

at low kinetic energies, a phase-dependent high-energy component with a pronounced cutoff, and the asymmetry pattern similar to the experiment, see Fig. 1g–i. The slightly more isotropic distribution in the experimental momentum map can probably be attributed to additional scattering effects, for example, owing to a finite surface roughness of the experimental nanoparticles (see transmission electron microscopy and high resolution transmission electron microscopy images in the Supplementary Information), which are not accounted for in the modelling. The disappearance of the asymmetry oscillations with CEP around 47 eV coincides well with the energy cutoff, see Fig. 1h and i, and is in good agreement with the experimental cutoff value. The higher amplitude of the asymmetry parameter in the calculations as compared to the experiment, in particular towards higher kinetic energies, may in part be attributed to the presence of background in the experimental data: when the signal from nanoparticles equals the background level in the experiment, the measured asymmetry amplitude would be reduced by a factor of two.

For a detailed analysis of the physics described by the model, Fig. 3 compares results from simulations with (1) the laser and polarization fields alone (left panel) to simulations with (2) the full potential, that is including the Coulomb term from free charges (right panel). In case (1), the CEP-averaged electron energy spectrum (black line) exhibits a rapid signal decay at low electron energies and a plateau-like high-energy feature, see Fig. 3a. Partial energy spectra from trajectories with only a certain number of collisions (scattering events) show that direct electrons (no collisions, red shaded area) produce the low energy feature and backscattered electrons (one or two collisions, blue shaded area) are dominant in the high energy region, similar to atomic high-order ATI. The remaining multiply-scattered electrons give an additional nearly exponentially decaying contribution that vanishes in the high-energy region. The cutoffs of direct and backscattered electrons are at about 4 and $30U_p$, in fair agreement with the modified classical atomic cutoffs $2\tilde{\alpha}^2 U_p = 4.74U_p$ for direct and $10\tilde{\alpha}^2 U_p = 23.72U_p$ for rescattered electrons ($2U_p$ and $10U_p$ in the atomic case), where $\tilde{\alpha} = 1.54$ is the field enhancement factor at the poles of the nanoparticle (see Fig. 3a inset, for more details see the Supplementary Information). The approximately 30% higher backscattering cutoff in our model expresses that electrons are born with an initial displacement to the residual ion, that is, at the tunnel exit, which is neglected in the classical $10U_p$ cutoff law. However, a comparison with the experimental results shows that the simulations with the laser and polarization field alone predict a too strong signal from direct electrons at low energies (see Figs 1e and 3a) and energy cutoffs for backscattering electrons well below the experimental values (Fig. 2).

These discrepancies are almost fully resolved when taking into account the Coulomb field from liberated electrons and residual ions at the surface of the nanoparticle (Fig. 3b). In this case

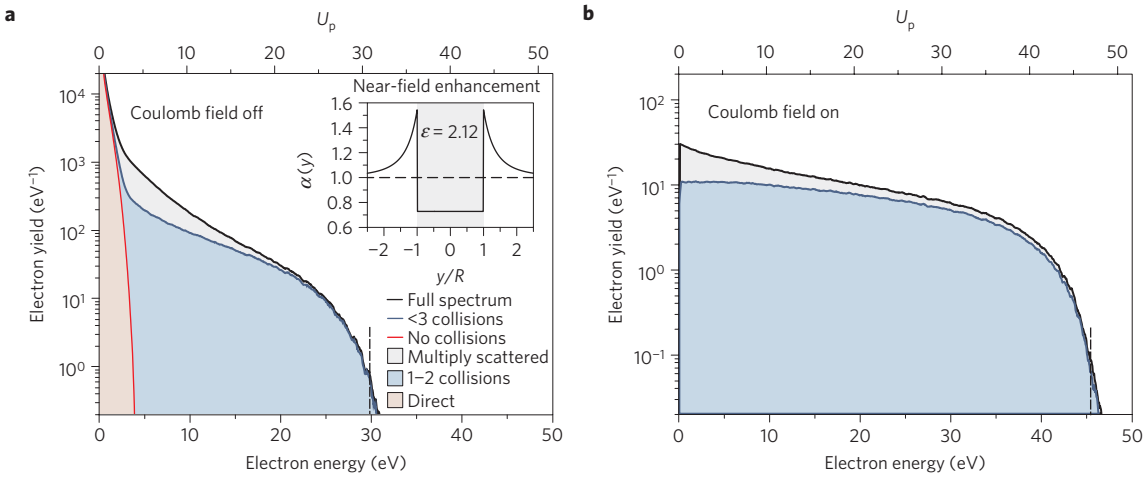

Figure 3 | Calculated electron energy spectra. a,**b**, Electron energy spectra from SiO_2 nanoparticles (diameter: 100 nm) for excitation with 5 fs pulses at 720 nm and $I_0 = 2 \times 10^{13}$ W cm^{-2} calculated without (**a**) and with the Coulomb field from free charges (**b**). Corresponding CEP-averaged energy spectra (black line) are given in **a** and **b** together with partial energy spectra (red, blue) from trajectories with a certain number of collisions (as indicated). The inset in **a** shows the y-dependent dielectric field enhancement $\alpha(y)$. The cutoff energies W_{cut} of the electron spectra (vertical dashed lines) were determined using the condition $P(W_{cut}) = P(W_{cut}/2) \times 10^{-2}$.

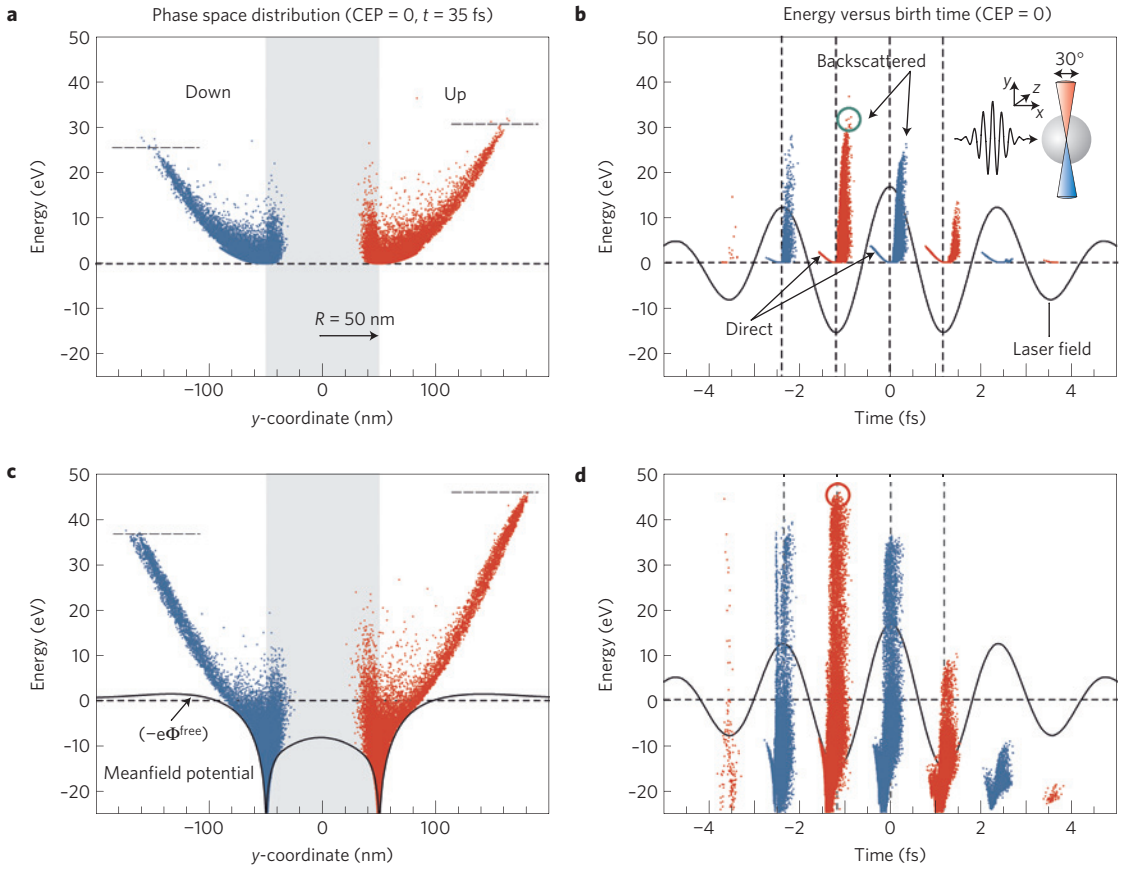

Figure 4 | Calculated electron emission from a SiO_2 nanosphere in a few-cycle laser field. a–d, Snapshots of the phase-space distributions (**a**,**c**) of single particle energies at a time $t = 35$ fs after the peak of the laser pulse and birth time analyses (**b**,**d**) for electrons emitted within a 30° cone (full opening angle) along the laser polarization vector (as indicated in the inset of **b**). The calculations were performed without (**a**,**b**) and with (**c**,**d**) the Coulomb field from free charges. In the calculations 100 nm diameter SiO_2 nanoparticles were excited by 5 fs pulses at 720 nm and $I_0 = 2 \times 10^{13}$ W cm^{-2}, and the CEP was set to $\phi = 0$. Green and red circles in **b** and **d** indicate typical fast trajectories.

the CEP-averaged spectrum is flatter, does not contain a direct electron feature, and the backscattering plateau extends up to $47U_p$, which is close to the experimental values (Fig. 2). Moreover, the intensity-dependent energy cutoffs show slopes similar to the experimental data. Figure 4 shows a more detailed analysis of the asymmetry and the time structure of the electron emission from the nanoparticles for the two model versions. Selecting a particular CEP ($\varphi = 0$), laser-aligned electrons show an asymmetric emission with different energy cutoffs for the up and down directions (cf. phase-space spectrum at 35 fs after the laser pulse peak in Fig. 4a for the case with the laser and polarization field alone). The corresponding final energy versus birth time analysis in Fig. 4b underlines the similarities with atomic ATI, that is, direct electrons have birth times before the field maximum of the corresponding half cycle, whereas the more energetic backscattering electrons show birth times after the field maxima (indicated by a green circle). The improved agreement between experiment and model that is achieved when taking the Coulomb field into account (Fig. 4c and d) can be traced back to the effect of the additional trapping potential arising from charge separation at the nanoparticle surface (Fig. 4c). Electron trajectories and their phase-space distributions are modified such that slow electrons that would be emitted directly in the absence of the trapping field remain bound and eventually return to the nanoparticle, and only sufficiently energetic backscattered electrons are able to escape. The energy versus birth time analysis in Fig. 4d reveals that the most energetic electrons (indicated by a red circle) are now born at or even slightly before the maximum of the electric field, a situation different from the classical rescattering picture. Two processes contribute to the increase in the cutoff energy: (1) the trapping field relaxes the birth time requirements for rescattering electrons, which promotes the acceleration process owing to higher return energies, (2) Coulomb repulsion of the created electron cloud results in further acceleration (for a detailed analysis see Supplementary Information).

Having identified the important mechanisms of electron acceleration near dielectric nanoparticles, we return to a closer comparison with the experimental results. Because of the high nonlinearity of the ionization probability, the effect of focal volume averaging on the simulated cutoffs is rather small, see Fig. 2. This effect is more noticeable in the full momentum distribution, which contains weak contributions from direct electrons produced in focus regions with low intensity, where electron trapping is weak (Fig. 1g). The simulations predict a weak increase of the energy cutoffs with particle size, which is mostly attributable to a size-dependence of space-charge repulsion between escaping electrons (see Supplementary Information). The absence of a clear size effect in the experimental results may be ascribed to the limited statistics available when using thin nanoparticle targets and CEP-stabilized few-cycle laser pulses, motivating further developments that allow one to increase the statistics in the experiments and include a larger size range of particles.

Conclusions and outlook

We have performed experiments on isolated SiO_2 nanoparticles in intense few-cycle waveform-controlled laser fields and observed

a large increase of the cutoff energy of emitted electrons when compared with atomic ATI. The cutoff in the electron energy spectra show a linear dependence on laser intensity in the range of $1–4.5\times10^{13}$ W cm^{-2}, with a cutoff at $(53.0\pm0.6)U_p$. A comparison with model calculations indicates that the large increase in the electron energy results from rescattering of previously tunnel-ionized electrons in the dielectrically enhanced near field of the nanoparticle surface and the trapping potential produced by residual ions and other free electrons in the surface region. This novel electron acceleration process is unequivocally identified from our studies on dielectric nanoparticles. Several aspects of the mechanisms discussed here for nanosized particles could, however, also be of importance in dielectric nanofilms, structured dielectric surfaces, and composite nanostructures exposed to few-cycle laser fields. Furthermore, we expect the acceleration process to be applicable to other materials, including semiconductor and metal nanoparticles and nanotips[38], in strong few-cycle laser fields. The controlled motion of electrons on nanometre spatial and attosecond temporal scales with optical light fields is a prerequisite for the realization of lightwave nanoelectronics.

The results indicate that field propagation effects in the nanoparticles are still sufficiently small to justify a description of the laser and the polarization field in the dipole approximation. Experiments with larger nanoparticles, in turn, open a unique avenue for exploring the onsets of propagation effects, such as nanofocusing and field distortions, along with their implications for tailoring electron acceleration with nanosystems[39].

The enhanced and waveform-controlled electron acceleration near dielectric targets in intense few-cycle laser fields may have also important implications for studying recollision-induced processes, such as the generation of XUV pulses by means of high-harmonic generation in mesoscopic systems. Such systems can serve as a source of coherent and incoherent radiation with potentially higher cutoff energies[40]. The cutoff energy of the XUV pulses can be estimated from our calculations for 100 nm SiO_2 nanoparticles at an intensity of 2×10^{13} W cm^{-2} to be about $20U_p$ higher as compared with the atomic case.

The experiments were performed at relatively low field intensities, where the dielectric response of the medium is still linear and the resulting electrons are sufficiently low in energy (<120 eV) to be detectable by our set-up. Extension of the experiments towards higher laser intensities might lead to a regime where the instantaneous medium response is highly nonlinear in nature and exhibits novel properties. Time-dependent density functional theory calculations for SiO_2 have predicted the optical breakdown of this dielectric at about 10^{15} W cm^{-2} (ref. 41). Recent theoretical work has revealed that dielectric nanofilms can metallize in strong adiabatic fields at intensities even below the optical breakdown[42]. Increasing the intensity close to or beyond the damage threshold would still allow the measurement of the electron dynamics without any significant influence from the motion of the nuclei in the particle because of the short laser pulse duration. Free nanoparticles would be particularly advantageous for exploring the nonlinear regime, as they provide constantly fresh samples for each laser shot. Drawing a parallel with nonlinear optics, which opened up nonlinear spectroscopic applications, the nonlinear behaviour of (nano)materials in strong laser fields has great potential in innovating completely new photonic applications.

Received 8 November 2010; accepted 17 March 2011; published online 24 April 2011

References

1. Vasa, P., Ropers, C., Pomraenke, R. & Lienau, C. Ultra-fast nano-optics. *Laser Photon. Rev.* **3,** 483–507 (2009).
2. Stockman, M. I. Ultrafast nanoplasmonics under coherent control. *New J. Phys.* **10,** 025031 (2008).
3. Kim, S. *et al.* High-harmonic generation by resonant plasmon field enhancement. *Nature* **453,** 757–760 (2008).
4. Sukharev, M. & Seideman, T. Coherent control approaches to light guidance in the nanoscale. *J. Chem. Phys.* **124,** 144707–144708 (2006).
5. Furube, A., Du, L., Hara, K., Katoh, R. & Tachiya, M. Ultrafast plasmon-induced electron transfer from gold nanodots into TiO_2 nanoparticles. *J. Am. Chem. Soc.* **129,** 14852–14853 (2007).
6. Cavalieri, A. L. *et al.* Intense 1.5-cycle near infrared laser waveforms and their use for the generation of ultra-broadband soft-x-ray harmonic continua. *New J. Phys.* **9,** 242 (2007).
7. Goulielmakis, E. *et al.* Single-cycle nonlinear optics. *Science* **320,** 1614–1617 (2008).
8. Krausz, F. & Ivanov, M. Attosecond physics. *Rev. Mod. Phys.* **81,** 163–234 (2009).
9. Uiberacker, M. *et al.* Attosecond real-time observation of electron tunnelling in atoms. *Nature* **446,** 627–632 (2007).
10. Goulielmakis, E. *et al.* Real-time observation of valence electron motion. *Nature* **466,** 739–743 (2010).
11. Cavalieri, A. L. *et al.* Attosecond spectroscopy in condensed matter. *Nature* **449,** 1029–1032 (2007).
12. Stockman, M. I., Kling, M. F., Kleineberg, U. & Krausz, F. Attosecond nanoplasmonic-field microscope. *Nature Photon.* **1,** 539–544 (2007).
13. Baltuska, A. *et al.* Attosecond control of electronic processes by intense light fields. *Nature* **421,** 611–615 (2003).
14. Paulus, G. G. *et al.* Measurement of the phase of few-cycle laser pulses. *Phys. Rev. Lett.* **91,** 253004 (2003).
15. Kling, M. F. *et al.* Control of electron localization in molecular dissociation. *Science* **312,** 246–248 (2006).
16. Dombi, P. *et al.* Observation of few-cycle, strong-field phenomena in surface plasmon fields. *Opt. Express* **18,** 24206–24212 (2010).
17. Stockman, M. I. & Hewageegana, P. Absolute phase effect in ultrafast optical responses of metal nanostructures. *Appl. Phys. A* **89,** 247–250 (2007).
18. Dombi, P., Rácz, P. & Bódi, B. Surface plasmon enhanced electron acceleration with few-cycle laser pulses. *Laser Part. Beams* **27,** 291–296 (2009).
19. Irvine, S. E., Dombi, P., Farkas, G. & Elezzabi, A. Y. Influence of the carrier-envelope phase of few-cycle pulses on ponderomotive surface-plasmon electron acceleration. *Phys. Rev. Lett.* **97,** 146801 (2006).
20. Donnelly, T. D., Ditmire, T., Neuman, K., Perry, M. D. & Falcone, R. W. High-order harmonic generation in atom clusters. *Phys. Rev. Lett.* **76,** 2472–2475 (1996).
21. Bhardwaj, V. R., Corkum, P. B. & Rayner, D. M. Recollision during the high laser intensity ionization of C_{60}. *Phys. Rev. Lett.* **93,** 043001 (2004).
22. Fennel, T. *et al.* Plasmon-enhanced electron acceleration in intense laser metal-cluster ineteractions. *Phys. Rev. Lett.* **98,** 143401 (2007).
23. Shu, J. *et al.* Elastic light scattering from nanoparticles by monochromatic vacuum-ultraviolet radiation. *J. Chem. Phys.* **124,** 034707–034709 (2006).
24. Bresch, H. *et al.* Elastic light scattering from free sub-micron particles in the soft X-ray regime. *Faraday Discuss.* **137,** 389–402 (2008).
25. Skopalova, E. *et al.* Pulse-length dependence of the anisotropy of laser-driven cluster explosions: Transition to the impulsive regime for pulses approaching the few-cycle limit. *Phys. Rev. Lett.* **104,** 203401 (2010).
26. Mathur, D. & Rajgara, F. A. Communication: Ionization and Coulomb explosion of xenon clusters by intense, few-cycle laser pulses. *J. Chem. Phys.***133**, 061101–061104.
27. Springate, E., Aseyev, S. A., Zamith, S. & Vrakking, M. J. J. Electron kinetic energy measurements from laser irradiation of clusters. *Phys. Rev. A* **68,** 053201 (2003).
28. Kumarappan, V., Krishnamurthy, M. & Mathur, D. Asymmetric emission of high-energy electrons in the two-dimensional hydrodynamic expansion of large xenon clusters irradiated by intense laser fields. *Phys. Rev. A* **67,** 043204 (2003).
29. Fennel, T. *et al.* Laser-driven nonlinear cluster dynamics. *Rev. Mod. Phys.* **82,** 1793–1842 (2010).
30. Znakovskaya, I. *et al.* Attosecond control of electron dynamics in carbon monoxide. *Phys. Rev. Lett.* **103,** 103002 (2009).
31. Yang, B. *et al.* Intensity-dependent scattering rings in high order above-threshold ionization. *Phys. Rev. Lett.* **71,** 3770–3773 (1993).
32. Paulus, G. G., Nicklich, W., Xu, H., Lambropoulos, P. & Walther, H. Plateau in above threshold ionization spectra. *Phys. Rev. Lett.* **72,** 2851–2854 (1994).
33. Paulus, G. G. *et al.* Absolute-phase phenomena in photoionization with few-cycle laser pulses. *Nature* **414,** 182–184 (2001).
34. Busuladžić, M., Gazibegović-Busuladžić, A. & Milošević, D. High-order above-threshold ionization in a laser field: Influence of the ionization potential on the high-energy cutoff. *Laser Phys.* **16,** 289–293 (2006).
35. Kling, M. F. *et al.* Imaging of carrier-envelope phase effects in above-threshold ionization with intense few-cycle laser fields. *New J. Phys.* **10,** 025024 (2008).
36. Jacoboni, C. & Reggiani, L. The Monte Carlo method for the solution of charge transport in semiconductors with applications to covalent materials. *Rev. Mod. Phys.* **55,** 645–705 (1983).

37. Salieres, P. *et al.* Feynman's path-integral approach for intense-laser-atom interactions. *Science* **292,** 902–905 (2001).
38. Schenk, M., Krüger, M. & Hommelhoff, P. Strong-field above-threshold photoemission from sharp metal tips. *Phys. Rev. Lett.* **105,** 257601 (2010).
39. Liseykina, T. V., Pirner, S. & Bauer, D. Relativistic Attosecond electron bunches from laser-illuminated droplets. *Phys. Rev. Lett.* **104,** 095002 (2010).
40. Zaretsky, D. F., Korneev, Ph. & Becker, W. High-order harmonic generation in clusters irradiated by an infrared laser field of moderate intensity. *J. Phys. B* **43,** 105402 (2010).
41. Otobe, T., Yabana, K. & Iwata, J. I. First-principles calculation of the electron dynamics in crystalline SiO_2. *J. Phys. Condens. Matter.* **21,** 064224 (2009).
42. Durach, M., Rusina, A., Kling, M. F. & Stockman, M. I. Metallization of nanofilms in strong adiabatic electric fields. *Phys. Rev. Lett.* **105,** 086803 (2010).

Acknowledgements

The authors acknowledge W. Siu and K. J. Schafer for making their TSDE data available to us, M. Kübel for helping with the laser intensity calibration, and S. Watson for providing experimental support. We are grateful for support by the Max-Planck Society, the EU through a Marie-Curie Reintegration Grant and the ATTOFEL network, and by the DFG through the Emmy-Noether program, the Cluster of Excellence: Munich Center for Advanced Photonics (MAP), SPP1391 and SFB 450 as well as BMBF through the network PhoNa and grant nos: 05KS7KEA and 05K10KE2. M.F.K. acknowledges support from KAIN within the KSU-MPQ collaboration. T.F. and C.P. gratefully acknowledge financial support from the DFG within SFB 652/2. I.A. is grateful for support from the Higher Education Commission of Pakistan (HEC-DAAD 2006/11586). The work of M.I.S. and M.F.K. has been supported by grants from the Chemical Sciences, Biosciences and Geosciences Division of the Office of the Basic Energy Sciences, Office of Science, US Department of Energy. M.I.S. acknowledges support by BaCaTeC and the US–Israel Binational Science Foundation.

Author contributions

E.R. and M.F.K. conceived the experiment; S.Z., J.P., E.A., I.Z. and B.L. performed the measurements; C.G. synthesized and characterized the SiO_2 nanoparticles; S.Z., J.P., I.Z., M.J.J.V., M.I.S., F.K., E.R. and M.F.K. evaluated, analysed and interpreted the experimental data; F.S. and C.P. did FDTD calculations, and T.F. developed the theoretical model and performed the Monte Carlo trajectory calculations. All authors discussed the results and contributed to the final manuscript.

Additional information

The authors declare no competing financial interests. Supplementary information accompanies this paper on www.nature.com/naturephysics. Reprints and permissions information is available online at http://www.nature.com/reprints. Correspondence and requests for materials should be addressed to T.F., E.R. or M.F.K.